Image Reconstruction for a Novel Compton Scatter Tomograph

Alfred Hero, Anne Sauve and Tom Kragh
Dept. EECS, University of Michigan Ann Arbor, MI 48109-2122

Abstract

Single photon emission computed tomography (SPECT) is a widespread medical imaging technology which provides images of metabolic tracer distributions within the body by detecting gamma-ray emissions from decaying radioactive isotopes in the tracer. The Compton single photon emission tomograph (C-SPECT) is a new imaging technology under development at the University of Michigan which promises significantly higher sensitivity than standard mechanically collimated SPECT scanners due its use of fully 3D electronic collimation of Compton scattered gamma-rays. Since the C-SPECT scanner generates extremely large data sets, and since the gamma-ray emission and detection processes are governed by the statistical physics of nuclear interactions, the theory of large scale statistical signal and image processing must play a significant role in the development of this new technology. In this paper we will summarize results on the application of estimation theoretic lower bounds and image reconstruction to a C-SPECT system.

1 Introduction

Radionuclide imaging is one of the most widespread medical imaging modalities due to its ability to map concentrations of radiolabeled metaboloids in the human body. Unlike X-ray CT and Ultrasonic imaging, which image anatomical structures, radionuclide imaging can determine metabolic function of an organ by quantifying its uptake of a radioactive isotope. The wide array of biochemicals that can be efficiently labeled with radiactive isotopes has greatly enhanced the number of clinical applications of radionuclide imaging including detection of lesions in brain, thyroid, heart, and bone. Tomographic methods have enabled radionuclide scanners to render images of 3D radionuclide concentrations inside the body based on projections of the emitted photons onto 2D photosensitive detector surfaces. These methods are collectively known as Emisson Computed Tomography (ECT) methods. The prospect of obtaining true 3D spatial information has both enhanced the utilization of ECT and created momentum to develop new scanners that have higher spatial resolution and capture a larger proportion of the emitted photon flux.

Today the two common tomographic radionuclide imaging modalities are Single Photon Emission Computed Tomographs (SPECT) and Positron Emission Tomographs (PET). The first SPECT instrument was developed in 1963, a decade before the more commonly known CT X-ray scanners. SPECT systems are low cost and radiopharmaceutical labeling compounds are safe, varied, and convenient to administer. SPECT systems detect a single photon emission from a decaying radioisotope and require mechanical collimation to obtain acceptable spatial resolution at the expense of sensitivity (reduced photon flux). Mechanical collimation refers to the insertion of a perforated lead shield between the radioisotope source, i.e the patient, and the detectors in order to reduce the angular uncertainty in the direction of arrival of detected photons (see Fig. **??**). Although mechanical collimation is simple and relatively inexpensive to implement, it has the fundamental drawback that it has poor sensitivity. Even in the case of the pinhole collimator, and without considering attenuation and scatter effects, only about 10^{-4} of the emitted photons are detected. On the other hand PET systems detect two antipodal emitted photons in coincidence, obtaining higher spatial resolution per photon than SPECT. However, PET scanners are much more expensive than SPECT scanners and the radiolabeling chemistry is less

[1]This work was supported in part by U.S. DHHS NIH grants R01-CA-32846 and RO1-CA-54362.

well developed, i.e. only a few useful positron emitting radio-pharmaceuticals are currently available.

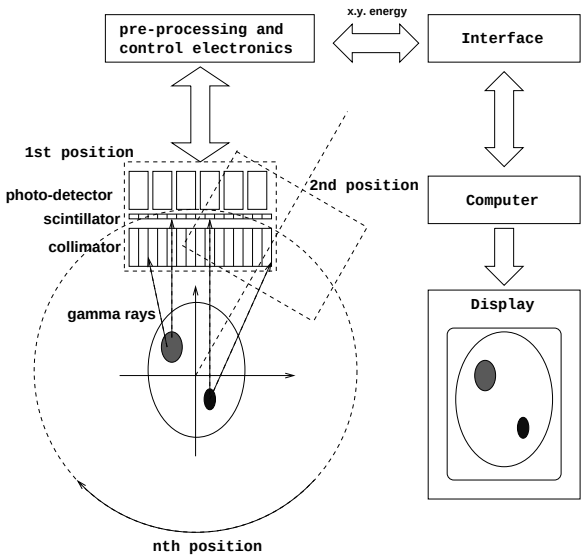

Figure 1. Block diagram of a SPECT system with rotating gantry.

In the past twenty five years, efforts have been made to develop Compton Single Photon Emission Computed Tomography (CSPECT) cameras for medical imaging that can overcome the poor sensitivity of SPECT systems [**?**]. The Compton SPECT camera consists of a pair of position sensitive detectors, a Compton scatter detector and a detector to absorb the scattered photons. The energy and position information from these detectors gives information about the energy, position, and incident direction of the incoming γ-ray. Such electronic collimation has superior sensitivity relative to conventional mechanical collimation since it passes all incident photons regardless of their direction of arrival. However, electronic collimation multiplexes all incident photon directions onto the detector surface which may require a more complicated reconstruction algorithm to recover spatial resolution. An effort led by Dr. W.L. Rogers at the University of Michigan has developed a CSPECT system shown in Fig. **??**. This system uses a conventional SPECT ring scanner, called SPRINT, for detection of the scattered photon and a solid state Compton scatter detector placed in the center of the ring. Two fundamental questions that we have been addressing are:

1. Does CSPRINT offer a performance improvement? That is, can one recover enough resolution from the CSPECT projections outperform standard SPECT in terms of image reconstruction pereformance?
2. If such performance improvement exists can practical image reconstruction algorithms be implemented?

Figure 2. *CSPRINT System consists of a set of 11 detector modules arranged around a ring, SPRINT, to detect Compton scatter photons passing through a solid state silicon Compton scatter detector placed in the center of SPRINT.*

While substantial advances have been made in the past decade on CSPECT in general [**?**] and CSPRINT in particular [**?**, **?**, **?**, **?**], as yet answers to these questions are incomplete. This paper discusses current directions that we are taking to answer these questions.

2 CSPECT System

The Compton collimator consists of a position sensitive solid state detector ($\det_1$) with high energy resolution. This detector is paired with a second position sensitive detector, $\det_2$, which can be a scintillation camera with lower energy resolution. The γ rays from a point source at position $\underline{x}$ that reach $\det_1$ are Compton scat-

tered by the solid state detector, $\det_1$ (Fig.**??**). The scattered photons are then detected by the second detector in coincidence with the events in $\det_1$. Assuming the photon is scattered by a single electron at rest, i.e. having zero momentum, the energy $\Delta E = E_o - E$ (in KeV) deposited in $\det_1$ increases as a function of the scattering angle θ according to the Compton scatter relation [**?**]

$$\Delta E = E_o \frac{\frac{E_o}{511}(1-\cos\theta)}{1+\frac{E_o}{511}(1-\cos\theta)}$$

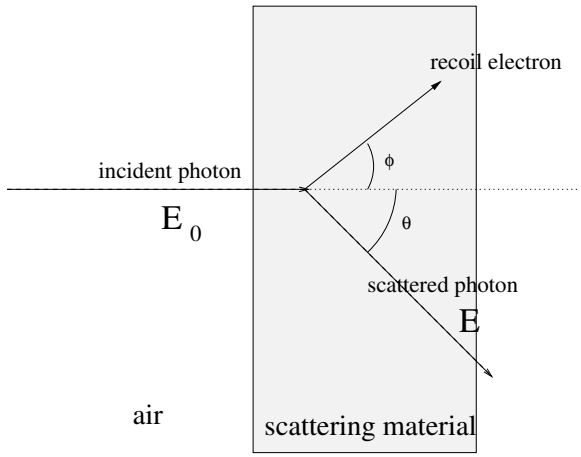

Figure 3. *Compton scatter of an incident photon of energy E_o by a solid state scattering material. The incident photon scatters off of an atom in the material producing a scattered photon of energy E at angle θ and a recoil electron of energy $E_o - E$ which generates a detectible current in the solid state material.*

The Compton scatter relation provides a one-to-one map relating measured energy ΔE to scatter angle θ. Since the vector describing the scattered photon is known from the position of interaction of the incident photon on the solid state detector and the position of interaction of the scattered photon on the SPRINT detector, the direction of the incident photon can be identified up to a conical ambiguity. With perfect energy resolution and no Doppler broadening, the measured energy of the recoil electron determines the scatter angle θ and the emitted photon must lie on the surface of a cone centered along the axis described by the segment $\det_1$-$\det_2$ and with conical angle θ.

A more accurate model includes Doppler broadening due to electron momentum. Doppler broadening smears out the one-to-one Compton relation in a manner specified by the joint probability density of θ and ΔE through the Klein-Nishina formula [**?**]. In this case only the conditional distribution of the Compton scatter angle given ΔE can be determined by the energy measurement leading to conical ambiguity on a cone with finite thickness proportional to the conditional standard deviation of the conditional density [**?**].

3 Statistical Model

An injected radio-isotope emits photons according to a space-time Poisson process with intensity $\theta(\underline{x}, t)$, where $\underline{x} \in \mathbf{R}^3$ and $t \in [0, T]$ the scan time interval. We restrict attention here to the case that the intensity is constant over the scan interval so that θ is independent of t. The probability that an emitted photon at position $\underline{x}$ is detected in the dth cell on a detector surface is $p(d|\underline{x})$ which is the solid angle between the cell surface and the photon emiission location. With m detector bins and n emission cells we define the vector $\underline{y}$ of detected counts over these bins and the vector $\underline{x}$ of emitted counts over the emission cells. Elements of $\underline{y}$ are detected counts in each bin, known as the projection data, and are Poisson distributed with intensity given by the corresponding elements of the vector

$$\underline{\mu} = T\underline{\theta},$$

where T is an $m \times n$ matrix of transition probabilities, also known as the system matrix and $\underline{\mu} = E[\underline{y}]$ and $\underline{\theta} = E[\underline{x}]$ are the detector and emission count rates, respectively.

4 Reconstruction Algorithms

We are taking two approaches to image reconstruction: simplification of the system matrix and implementation of iterative ML reconstruction algorithms. What makes image reconstruction for CSPECT a hard problem is that the Poisson likelihood function is very difficult to maximize over the unknown intensity $\underline{\theta}$. This is due to the very large dimension of the system matrix T

which has a number of columns (image pixels) on the order of 10^6 or more and a number of rows (detector bins) on the order of 10^9 due to the large number of energy bins and spatial bins which must be created for the detected data. Furthermore, as the matrix T is not sparse, storage of its 10^{15} elements is impractical. To further complicate the issue T is typically ill-conditioned, and the estimates of $\underline{\theta}$ must be constrained to be smooth and positive.

In [**?**] we showed that the Compton system matrix T could be approximated by the product of block circulant matrices, diagonal matrices, and sparse interpolation matrices, effectively reducing the forward projection computation from $O(n^2)$ operations to $O(nlogn)$ operations where n is the number of pixels in the source domain. As explained in [**?**] this computation requires rebinning the set of samples of the detected coincidence pairs onto hemispherical surfaces and implementing a fast 3D volumetric interpolation.

In particular we showed that the forward projection for a given energy and tomographic rotation angle Φ has the compact representation

$$\mu_{E,\Phi} = \mathbf{W}^H_{n\times n}\tilde{\mathbf{h}}^{x_0}_E \odot [\mathbf{R}\otimes\mathbf{I}_m]\mathbf{Q}_\Phi\lambda \qquad (1)$$

where $\mathbf{W}_{n\times n}$ is the 2D FFT matrix, $\tilde{\mathbf{h}}^{x_0}_E = \mathbf{W}_{n\times n}\mathbf{h}^{x_0}_E$ is the 2D FFT of the point response function of the Compton camera at a particular measured Compton energy E level, and x_0 an arbitrary origin in the object space, and $\odot$ denotes the element-by-element vector product.

By using a polyhedron approximation to the voxels induced by the intersected hemispheres and fast volumetric interpolation the matrix $\mathbf{Q}$ becomes sparse. Moreover, only the Fourier domain transfer function $\tilde{\mathbf{h}}_{Ej}{}^{x_0}$ and the l scalars ρ_i in R need be stored leading to reduction of storage requirements by several orders of magnitude. We are currently investigating the use of these approximations to the transition matrix in a list mode EM maximum likelihood reconstruction algorithm in order to simplify each iteration of the algorithm.

5 Performance Assessment

In order to understand the estimator performance limitations associated with different object intensities, projection geometry configurations, image reconstruction algorithms, and parameter estimators, a thorough systems evaluation is required. For a clean analysis, a tool is needed which can separate the effects of reconstruction algorithm limitations from imaging system limitations while capturing the intrinsic tradeoffs between reconstructed resolution, estimator bias, and estimator variance. As explained below, during the uniform Cramèr-Rao bound (UCRB) was developed for this purpose in [**?**] and has been applied to tomographic imaging and other applications including CSPRINT [**?**, **?**, **?**]. The UCRB captures the fundamental bias-variance tradeoff by specifying the variance of the optimal bias constrained estimator, where estimator bias was characterized by estimator bias gradient norm (Euclidean l_2 norm). Since the bias gradient of an estimator is closely related to the average difference between the ideal dirac point spread function (PSF) and the estimator's mean PSF [**?**], the l_2 norm of the bias gradient suggests itself as a reasonable measure of estimator spatial resolution. Indeed, an estimator with zero bias gradient norm has a dirac PSF and hence perfect spatial resolution.

One of our principal efforts has been to understand the meaning of the bias gradient length and its relation to common tomographic reconstruction measures such as spatial resolution and/or sensitivity. The k-th component of the bias gradient specifies the influence that a given parameter, e.g. a particular object pixel intensity θ_k, has on the mean of the estimator of a function $t(\theta)$ of the intensity vector θ. A large value indicates that the estimator will be highly sensitive to changes in the k-th object pixel θ_k. Such sensitivity can occur even when the function $t(\theta)$ to be estimated is independent of θ_k, e.g. estimation within an ROI can be sensitive to a pixel value outside the ROI. The length $\delta = \|\underline{d}\|$ of the bias gradient is a measure of the overall non-removable estimator bias.

The uniform CR lower bound applies to all estimators $\mathbf{T}$ whose bias gradient length is less than or equal to δ. Therefore, for each δ, $B(\delta)$ provides a uniform lower bound on the error variance governing a large class of estimators. The plot of the lower bound over δ gives a curve $\{(\delta, B(\delta)) : \delta > 0\}$ which lower bounds the error of any estimator plotted as a point on the bias-variance plane. It was shown [**?**] that in general the uniform bound will be tight when an efficient unbiased estimator exists for estimation of $t(\theta)$. It has also been shown that the quadratically penalized maximum likelihood estimator virtually attains the UCRB for appropriate choice of

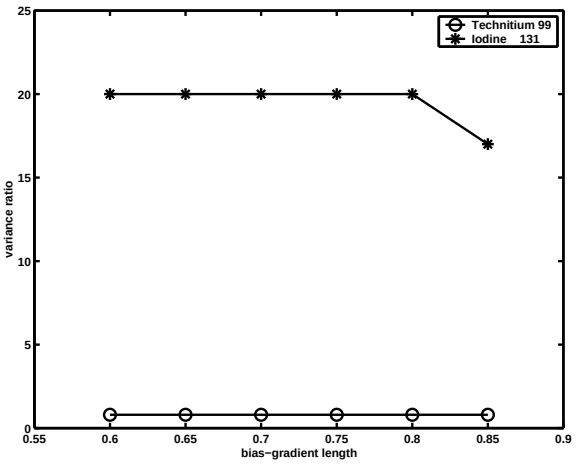

Figure 4. The ratio of UCRB variance ($\text{var}_{CSPRINT}/\text{var}_{SPRINT}$) at two different energies (courtesy of C.-H. Hua [**?**]).

penalty [**?**, **?**, **?**] for both Poisson and Gaussian image reconstruction problems.

Figure **??** shows the results of UCRB calculations performed by our co-workers [**?**] for comparing CSPRINT to conventional SPRINT for two differnet radiolabel compounds Technicium-99 (140.5KeV) and Iodine-131 (364.4KeV). Several system approximations were used which are explained in [**?**]. The range of bias gradient lengths studied correspond to the bias of smoothed reconstructed images typical in nuclear medicine. Shown are the ratio of the SPECT vs CSPRINT UCRB for six different values of bias gradient. The result suggests that while there is a loss in attainable variance performance at 140.5KeV there is a factor of 20 advantage of CSPRINT at 364.4KeV. The issue of attainment of this bound is still an open problem. We are currently working on extensions to the UCRB which explicitly account for system resolution by using an appropriate norm in the bias gradient constraint which is used to compute the UCRB [**?**].